DETECTION AND MEASUREMENT OF DENSITY FLUCTUATIONS INDUCED BY A MAGNETOHYDRODYNAMIC FORCE IN A SUPERSONIC BOUNDARY LAYER

A THESIS

Presented in Partial Fulfillment of the Requirements for Graduation with

Distinction in the Department of Mechanical Engineering at

The Ohio State University

By

Michael E. Cundy

The Ohio State University

2005

Abstract

This project is producing experimental data which can define the influence of electro-magnetic fields on density fluctuations (turbulence) in a supersonic boundary layer. By investigating the behavior of density fluctuations in the boundary layer under certain conditions, this Air Force funded project will aid in the development of advanced supersonic vehicles. Experiments have been performed with nitrogen gas and air. First, gas is emitted into a M=3 wind tunnel and ionized using an RF power supply. A DC voltage is then applied to draw a transverse current in the flow. A 1.5 T magnetic field is crossed with the DC field, which results in the Lorentz force acting on the free electrons and the positive ions in the flow. The direction of the force can be upstream or downstream, depending on the experimental configuration. Inherent turbulence is modified in both conditions. An accelerating force has shown to reduce density fluctuations by 5-10%, while a decelerating force has shown to increase density fluctuations by approximately the same amount. Currently, experiments are being performed to determine the flow regime in order to supplement these results. A Laser Differential Interferometer (LDI), which I have constructed, is used to measure the density fluctuations. This device, in which a laser beam passing through the boundary layer (probe beam) is combined with a second laser beam passing through the free stream (reference beam), creates a time dependant interference signal which is a function of the average density difference between the two paths. The resulting experimental data is processed using Fourier Transform techniques.

Acknowledgments

I would like to cordially thank each person who has helped me along this path, which has been a truly unforgettable experience. I would first like to thank my older brother Chris; if he had not participated in research as an undergraduate and exposed me to his work, I would not have pursued this project. I would like to thank my parents for their love and support. I am very grateful that Dr. Lempert and Dr. Adamovich gave me the opportunity to work on this project. They have helped me greatly along the way, and I would like to extend my sincere appreciation to them as well. Also, I would like to thank the members of my research group that have assisted in performing experiments and maintaining the experimental apparatus.

This research has been supported by the AFOSR under grant F49620-02-1-0164, Phase II SBIR grant F33615-01-C-3112 of Air Vehicles Directorate of AFRL, and by the National Science Foundation (NSF) Division of Plasma Physics.

Table of Contents

Introduction

Flow control through the use of magnetohydrodynamic forces continues to draw considerable interest in the aerospace domain. This technology has potential applications in areas such as supersonic flow control, supersonic air-breathing propulsion, and for development of novel supersonic ground testing facilities. The scope of this research lies in the supersonic flow control realm.

Magnetohydrodynamics (MHD) is defined as the study of the interaction of conducting liquids or gases and magnetic fields. It can be more easily understood as the Lorentz force effect in a fluid, except that the charged particle is an electrically charged fluid. MHD experimentation is largely guided by, or constrained by the level of conductivity in the flow. Recent experiments in a salt water boundary layer, a relatively conductive fluid, have demonstrated the ability to significantly amplify and reduce the turbulence intensity in the flow [1]. The conductivity in a low-temperature supersonic air or nitrogen flow must be induced, which is a challenging task. In order to produce an MHD effect large enough to generate significant changes in the free stream flow enthalpy on a flow of this nature, attention is often drawn to the strength of the electric and magnetic fields. High power electromagnets must be used in such cases. However, this research is concerned with the use of relatively small MHD forces that may be strategically applied near early instability waves in the boundary layer. These forces may be realized by using relatively inexpensive permanent magnets. MHD forces of this magnitude may also be applied to reduce boundary layer separation, since the flow enthalpy in these regions is very small.

This research can potentially be used in the design of advanced supersonic vehicles. MHD forces may be applied on the wing of a jet to delay the laminar to turbulent transition point, which would reduce the friction drag on the wing. Alternatively, MHD forces may be applied on the walls of the combustion chamber to enhance air/fuel mixing, which would improve combustion efficiency.

Laser Differential Interferometer

Introduction

The Laser Differential Interferometer (LDI) is a high precision, non-intrusive optical measurement system capable of measuring relative density in a flow field. In this system, a single beam is split into a reference and a probe beam. The beams pass through regions of the flow with different densities and are brought back together to produce a time-dependant interference signal that is a function of the average density difference between the two paths.

The speed of a light is dependant upon the index of refraction of the medium in which it travels according to the following formula:

$$v = \frac{c}{n} \qquad (1)$$

Where v is the velocity of the light in m/s, c is the speed of light in a vacuum (approximately $3.00*10^8$), and n is the index of refraction of the travel medium. The index of refraction of air is directly related to its density according to the following formula:

$$n = 1 + 0.000278 * r \qquad (2)$$

Where r is the density of air in amagats. Turbulence in higher Reynolds number flows induces pressure and temperature fluctuations, which corresponds to density fluctuations. Thus, density variations have been related to the index of refraction of the flow medium.

The precise response time and bandwidth of the system have not been computed since experiments and crude calculations have revealed that the system is adequate for the measurement of density fluctuations in a supersonic boundary layer. Experimental examination of the LDI's bandwidth was limited by the measurable frequency range of the spectrum analyzer (102.5 kHz). A signal generator was connected to the spectrum analyzer and a sine wave was generated at several different frequencies between 0-102.5 kHz and the frequency response was found to be flat. The RC time constant was estimated to be 1 μsec using a terminating resistor value of 10 kO and an estimated capacitance value of the coaxial cable of 100 pF. This verifies that the LDI is capable of measuring the spectrum of density fluctuations examined in this work (0-102.5 kHz).

System Description

A schematic of the LDI is shown in Figure 1. The LDI uses a Coherent 632.8 nm plane-polarized Helium-Neon laser (model # 31-2025) with a beam diameter of approximately 1 mm. The beam first passes through a quarter-wave plate which is oriented such that the plane of polarization of the beam bisects the fast and slow axis. The resulting beam is circularly polarized. The beam then passes through a 25.4 mm diameter achromatic doublet convex lens with a focal length of +50 mm. This lens reduces the beam diameter in order to lessen adverse fringing effects in the next component of the system. The beam is then split at a 5° angle using an AR coated Wollaston prism (a polarizing beam-splitting prism). The beams now have orthogonal plane polarizations. The orientation of the first quarter-wave plate should be adjusted until both beams have the same intensity. A 50.8 mm diameter achromatic doublet convex lens with a +100 mm focal length is used to collimate the beams. After this lens is the test section of the device. The optical components in the second half of the LDI are essentially the same as the components used in the first half, but in reverse order. Another 50.8 mm diameter achromatic doublet convex lens with a +100 mm focal length directs the beams back towards each other, and an AR coated Wollaston prism overlaps the beams into a single, diverging beam. Note that this Wollaston prism is rotated 180° relative to the first Wollaston prism to overlap the beams, rather than split the beams into four. The reference and probe beams must enter the Wollaston prism with a separation angle of very close to 5° or else they will not remain overlapped in the rest of the system. A 25.4 mm achromatic doublet convex lens with a +50 mm focal length then collimates the beam. An aperture was placed in this section of the device to block stray reflected beams. Another quarter-wave plate is oriented such that the orthogonal plane-polarizations of the overlapping beams bisect the fast and the slow axis. Lastly, another AR coated Wollaston prism splits the overlapping beams and two high speed photodiodes measure the resulting intensity [2].

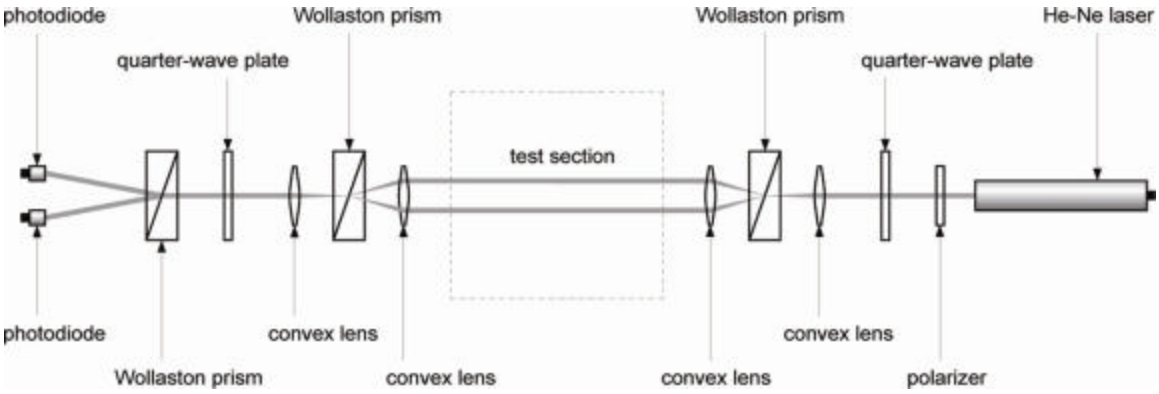

Figure 1: Schematic of the Laser Differential Interferometer.

The need for constant realignment and tuning to evaluate density fluctuations at different areas of the flow and to align the LDI for use with other wind tunnels requires that rotary mounts hold the quarter-wave plates and the Wollaston prisms.

This system can be adapted to other experimental setups. The laser beams can be redirected using front faced mirrors at any section of the LDI. The beam separation can be adjusted by replacing the convex lenses that surround the test section. The reference and probe beam diameters can be adjusted by replacing the smaller convex lenses.

Signal Processing

Since the oscilloscope and spectrum analyzer are sensitive to voltage signals, terminating resistors were installed to generate a voltage from the photodiode current output signals. Variable terminating resistors with 1 kO, 10 kO, and 100 kO settings were used. The magnitude of these resistors manages the systems sensitivity - bandwidth characteristics. Both terminating resistors were arbitrarily set to 10 kO since that resulted in an instrument with sufficient sensitivity and bandwidth.

The photodiode signals are sent to an oscilloscope to verify that the beams are overlapped and interfering with each other, and to a spectrum analyzer to measure the spectrum of the relative density fluctuations. The signals are differenced in the spectrum analyzer, and the resulting signal is processed using the fast-Fourier transform feature. The spectrum was measured over a 102.5 kHz span. The typical setting for FFT lines was 100, and the signal was taken and averaged 500 times per test. Each measurement took approximately 3-5 seconds. The first few data points are not useful because they

merely contain the differenced DC components of the signal, so they were not included in the plots for clarity purposes.

The resolution and range of measurement of the LDI can be estimated using its baseline spectrums, flow spectrums, and theoretical calculations. The baseline spectrums in Figure 2 indicate that the DC signal level, which corresponds to complete constructive interference, is approximately 15 dB, while the high frequency level settles at approximately -80 dB. Since the high frequency level is about 95 dB below the DC level and complete constructive interference corresponds to a phase shift of 1 fringe, the resolution of the LDI is estimated to be 1/56,000 of a fringe, or 0.01 nm. It can also be seen in Figure 2 that the high frequency density fluctuation levels midway through the boundary layer, which is the test location in this work where the turbulence is greatest, is approximately 40 dB below the DC level. From this, the density fluctuations are estimated to be 1/100 of the mean density. Using formulas 1 and 2 with a wind tunnel height of 4 cm and the estimated density fluctuation level, the upper range of LDI measurement is approximately 8.4 nm, or close to 1/100th of a fringe.

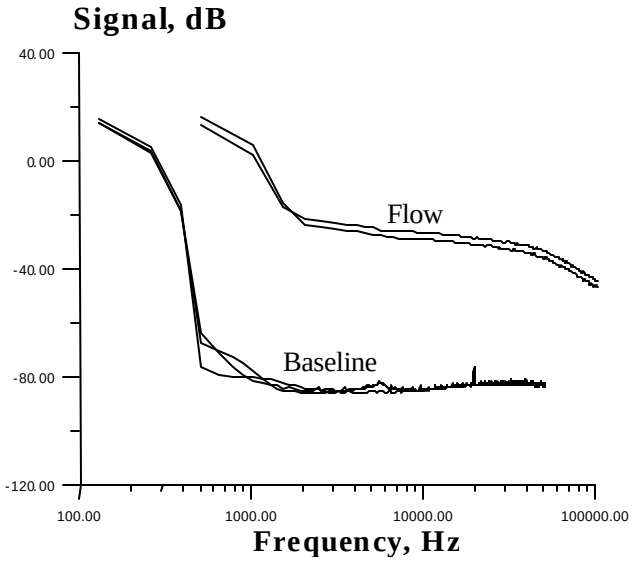

Figure 2: Three LDI baseline spectrums and two LDI flow spectrums with a stagnation pressure of 250 torr and the probe beam located midway through the boundary layer. The high frequency baseline spectrums appears to be approximately 95 dB below the DC portion, while the high frequency flow spectrums appears to be approximately 40 dB below the DC portion. From this, the resolution and range of measurement of the LDI are estimated.

Signal Validation

The presence of interference in the photodiode signals is verified by blocking one beam in the test section and viewing the resulting signal on an oscilloscope. When one beam is blocked in the test section, the other beam is essentially split in half and sent to the photodiodes, and a stable voltage is observed. This is because constructive and destructive interference cannot occur with only one electromagnetic wave present. Another method of verifying the interference in the system was by placing a hot soldering iron close to one of the beams in the test section. As the ambient air is heated, the beams travel through regions of varying density. If the system is measuring density fluctuations, the signal will be convulsive because of air drifts carrying the heated air elsewhere.

Low frequency mechanical vibrations on the LDI and the wind tunnel do not affect the integrity of the high frequency signal. The calibration of the LDI is often verified by tapping a finger on the LDI's stand. This causes a difference in beam path lengths exceeding 2p by vibrating the optics, which results in interference. The peak-to-peak amplitude of the observed interference does not change as the force of the tapping increases or decreases; only the time between subsequent peaks changes. The varying time between subsequent peaks is expected due to the changing frequency of the large amplitude mechanical vibrations. The peak-to-peak amplitude should not increase with tapping levels since the maximum constructive interference occurs at path differences of 2pn, where n is an integer. Since the peak-to-peak amplitude did not decrease when the LDI's stand was tapped (hard enough to produce 2p path differences), it can be concluded that the beam overlap is not significantly affected by the mechanical vibrations. Note that the mechanical vibrations are essentially cropped from the LDI spectrum measurements because their frequencies are well below those of the density fluctuations in the boundary layer.

The affect of mechanical vibrations was also tested by dampening the vibrations of the wind tunnel while it was operating. The wind tunnel was held in a pair of hands to dampen the vibrations, and the measurements that were taken did not appear to differ from other measurements with similar configurations.

A typical boundary layer spectrum measured by the LDI at 250 torr stagnation pressure can be seen in Figure 3. This spectrum is consistent with boundary layer

turbulence spectrums measured in past experiments (see Figure 4), which validates the LDI's measurements.

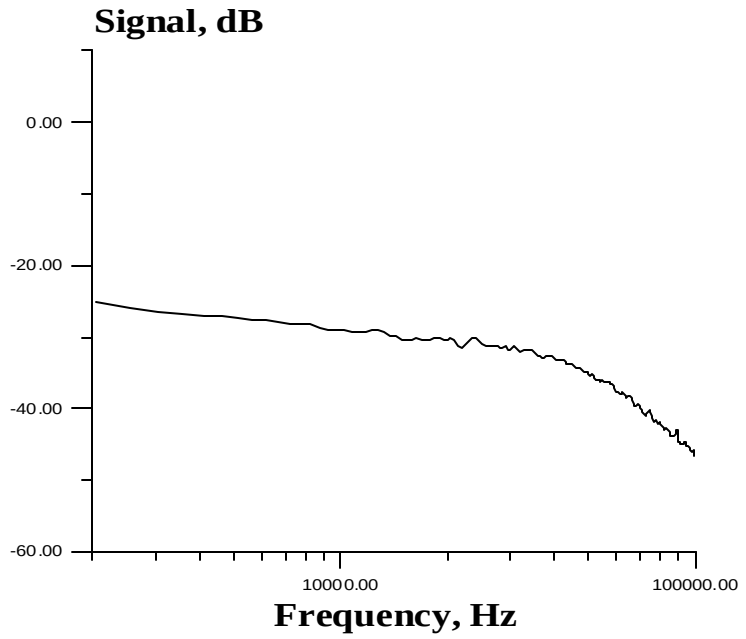

Figure 3: Typical boundary layer spectrum measured by the LDI. The stagnation pressure is 250 torr, and the probe beam is located midway through the boundary layer.

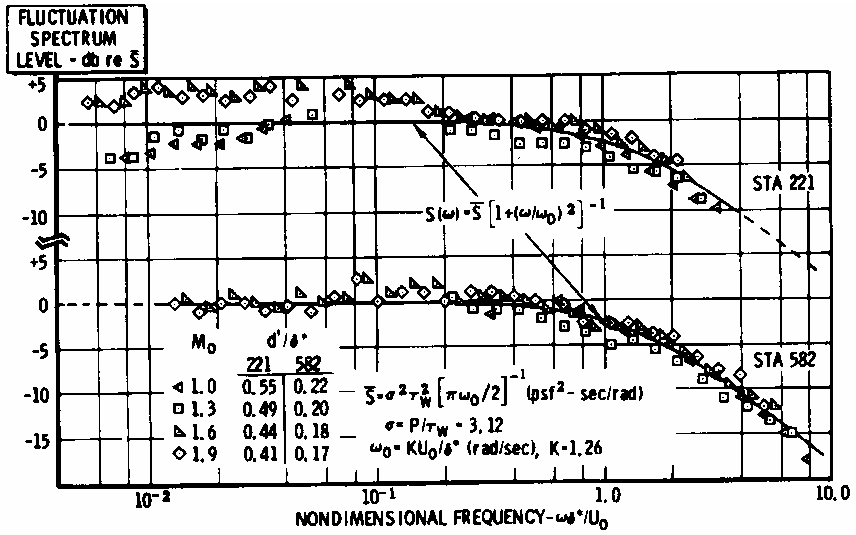

Figure 4: Pressure fluctuation spectra in a M=1.0-1.9 supersonic boundary layer. Flight measurements at 221 in and 582 in aft from the nose of a flight vehicle [3]

Experimental

Facility:

Experiments have been conducted in the Non-Equilibrium Thermodynamics Laboratories at The Ohio State University. A pressurized gas tank of air or nitrogen is connected to the wind tunnel assembly, which is connected to 1200 ft^3 dump tank that is pumped out by an Allis-Chalmers 1300 cfm rotary vane vacuum pump. The location of the wind tunnel with respect to the LDI can be seen in Figure 5.

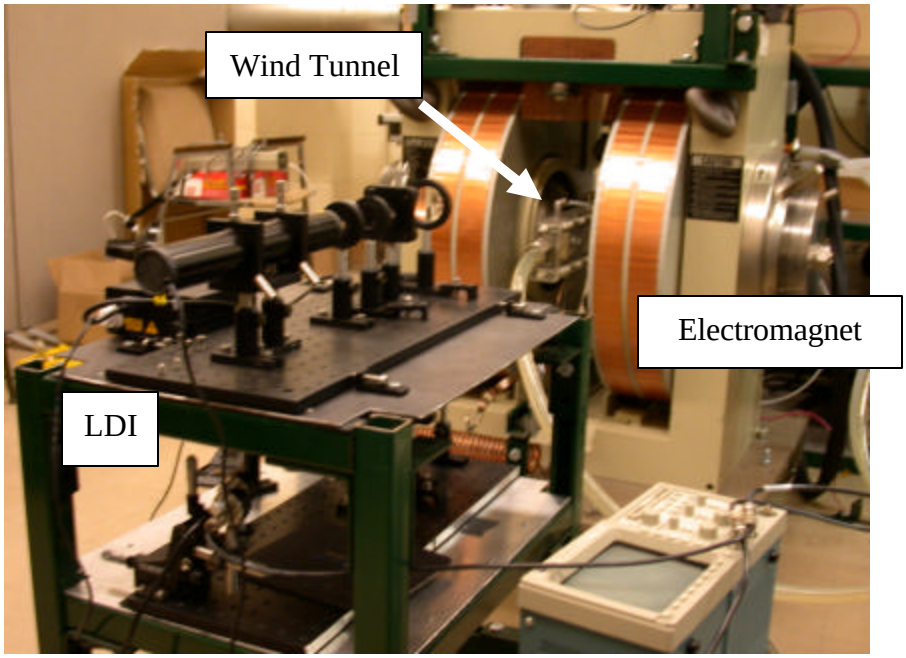

Figure 5: Picture of experimental setup

The MHD force is induced through the use of three electromagnetic fields. First, the flow is ionized using an RF power supply. A DC voltage is then applied to draw a transverse current in the flow. A 1.5 T magnetic field is crossed with the DC field, which results in the MHD force acting on the free electrons and the positive ions in the flow. The direction of the force can be upstream or downstream, depending on the experimental configuration. Figures 6 and 7 show side and top view schematics of the wind tunnel with the RF and DC electrode blocks installed. The location of the magnet poles with respect to these electrode blocks can also be seen in these figures.

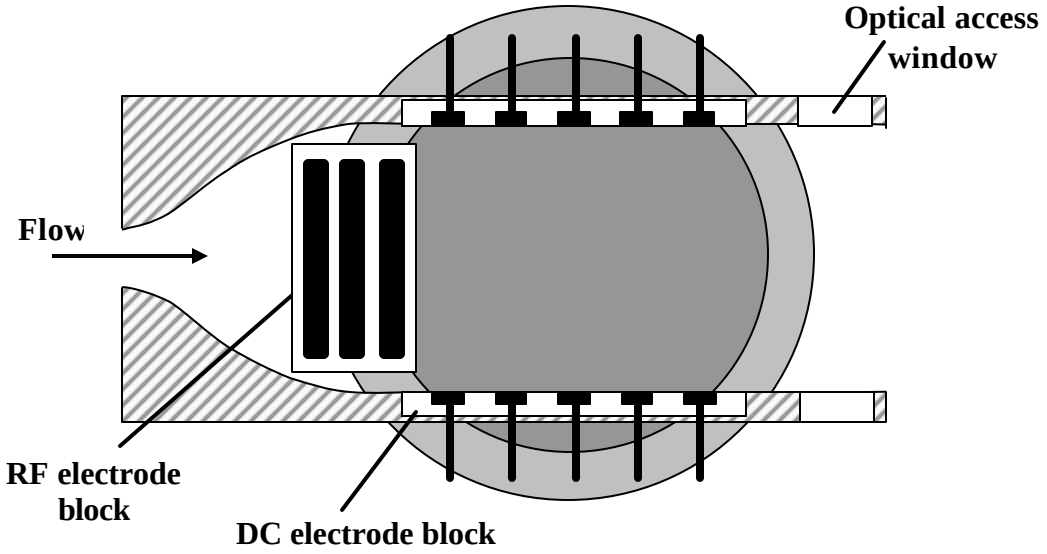

Figure 6: Side view schematic of the wind tunnel

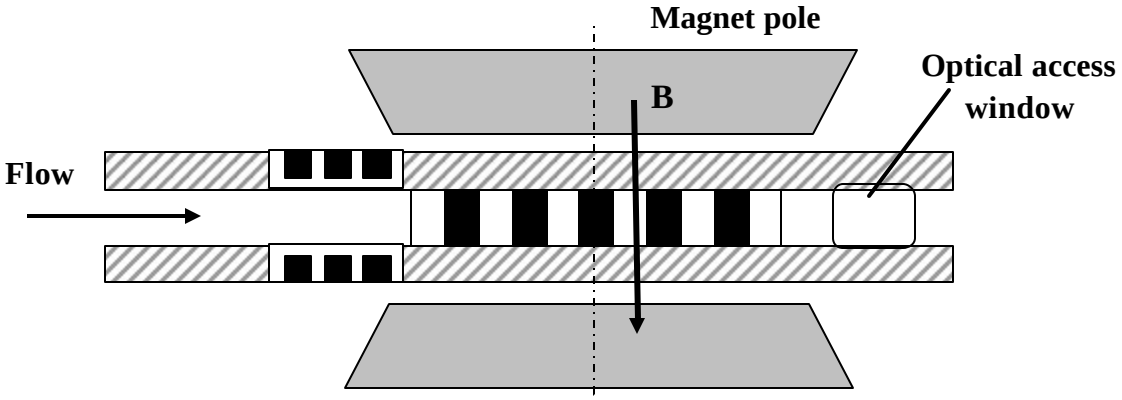

Figure 7: Top view schematic of the wind tunnel

Two transparent acrylic plastic wind tunnels have been constructed for the experiments. Figure 8 shows a side view of the first test section used in experimentation. Each wind tunnel measures 2 cm x 4 cm. Mach 3 flow is generated with nozzle throat dimensions of 9.5 mm x 20 mm. Figure 9 shows a close-up picture of the nozzle. The wind tunnels are equipped with three pressure taps that measure the plenum pressure and the static pressure in the test section and the diffuser. The boundary layer of interest is located on the larger dimension wall, which is vertical when the wind tunnel is installed. The boundary layers on the smaller dimension walls and their interaction with the boundary layer on the larger dimension wall is ignored. The primary difference between

the two wind tunnels is the location of the glass optical access windows and the location of the ionizing electrodes; the contours of the interior walls were manufactured by the same company according to identical specifications. The optical access windows are located on both the top and bottom walls of the wind tunnel (the smaller dimension walls). Glass windows are used to prevent attenuation and refraction of the LDI's reference and probe beams.

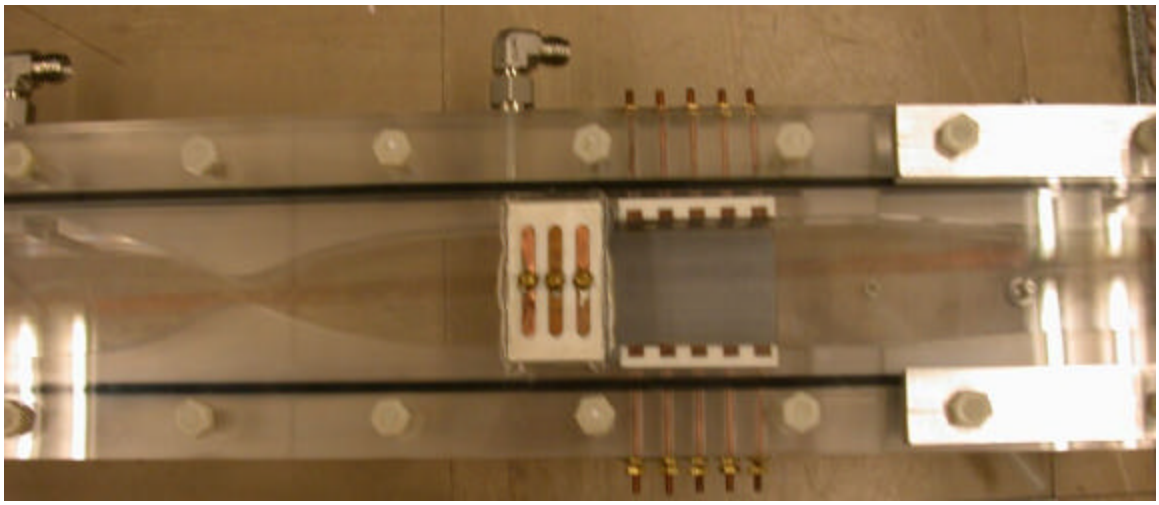

Figure 8: Side view of wind tunnel

Figure 9: Wind tunnel nozzle close-up

The flow is ionized using a 5 kW, 13.56 MHz Dressler power supply with an automatic impedance matching network. The ground and hot terminals are connected to electrode blocks 3 cm wide, which consists of three copper strips 35 mm long and 5 mm wide housed in high-temperature machinable mica ceramic (see Figures 6, 7, and 8). The edges of the copper strips are rounded to prevent high electric field concentrations, which can produce "hot spots" in the plasma. Dielectric ceramic layers have been installed between the electrodes and the flow to prevent secondary ionization, which greatly improves the stability of the plasma. Past experiments have shown this facility to produce stable and diffuse plasma [4]. The RF power supply was set to deliver 500 W to the electrodes during early experiments, and 1 kW to the electrodes in later experiments. The RF electrodes were cooled by running room air through the wind tunnel after each set of measurements with plasma flow. This maintained the temperature of the electrodes within a reasonable range and also prevented the test section from melting. Very good impedance matching was achieved, with roughly 5 % of the power reflected back. A picture of the afterglow can be seen in Figure 10.

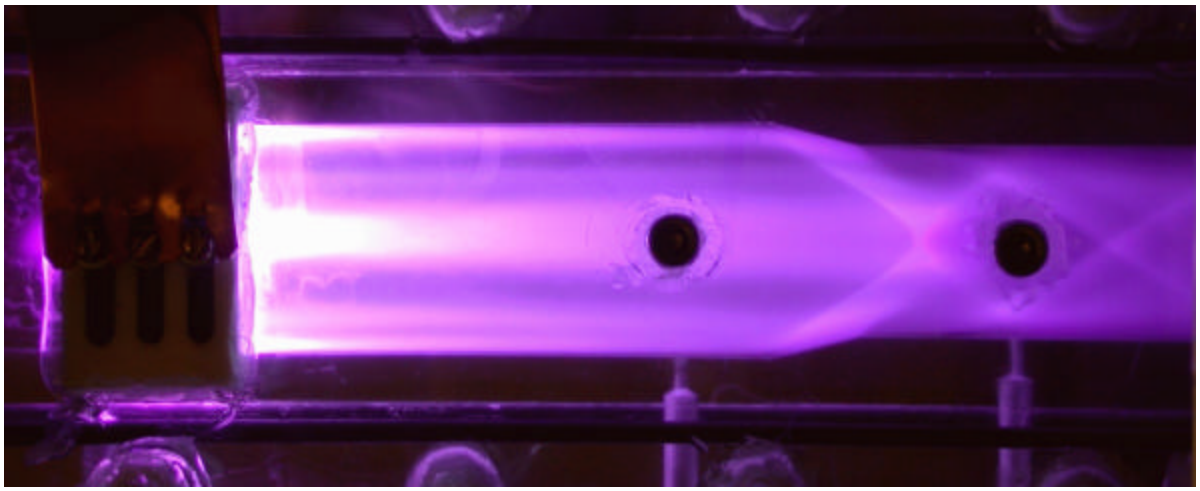

Figure 10: Plasma afterglow in a mach 3 flow with a 250 torr stagnation pressure

The magnetic field was created using a GMW water cooled electromagnet capable of generating up to a B=3.5 T steady state magnetic field. The 15 cm diameter poles were separated by approximately 6-7 cm to accommodate the wind tunnel

assembly. At this separation, the magnet can generate up to a B=2 T magnetic field. Typical experiments were operated with a B=1.5 T magnetic field. Figures 6 and 7 show the location of the magnet poles with respect to the major components of the wind tunnel.

The electric field was created using a DEL 2 kV / 3A DC power supply that was operated in voltage stabilized mode, with a 1-2 kO ballast resistor. The power supply was connected to two 50 mm x 20 mm electrode blocks that were flush mounted in the top and bottom walls of the test section (see Figure 6, 7, and 8). Each electrode block consists of five copper electrode strips 5 mm x 20 mm, with the smaller direction oriented axially, housed in a high-temperature aluminum bisilicate ceramic material. The sectioned electrode design allows for the ability to produce transverse and axial DC electric fields; however, the sectioned electrodes were shorted and only transverse DC electric fields were used in this work. Experiments were conducted with electric field strengths of 500 V/cm, 1000 V/cm, and 1500 V/cm.

Figure 11 shows how the LDI is integrated into the experimental setup. Two front faced mirrors were used in order to circumvent the obstructions of the electromagnet fixture. The LDI beams enter the magnet fixture horizontally and are reflected downwards off of a mirror oriented at 45° with respect to the horizontal. The beams pass through the wind tunnel and are then reflected horizontally off of another mirror oriented at 45° with respect to the horizontal and exit the magnet fixture. The second half of the LDI, or the receiving end, was placed on the shelf immediately below the shelf that supported the first half (see Figure 5). All of the mounts, bolts, and brackets used to secure the mirrors were fabricated out of aluminum to minimize interaction with the magnetic field during experiments. Because magnetic interaction can steer the LDI signal, the magnet was powered on for several minutes before measurements were taken in order to ensure that the field had reached steady state and that elastic deformation of the mounting equipment had discontinued.

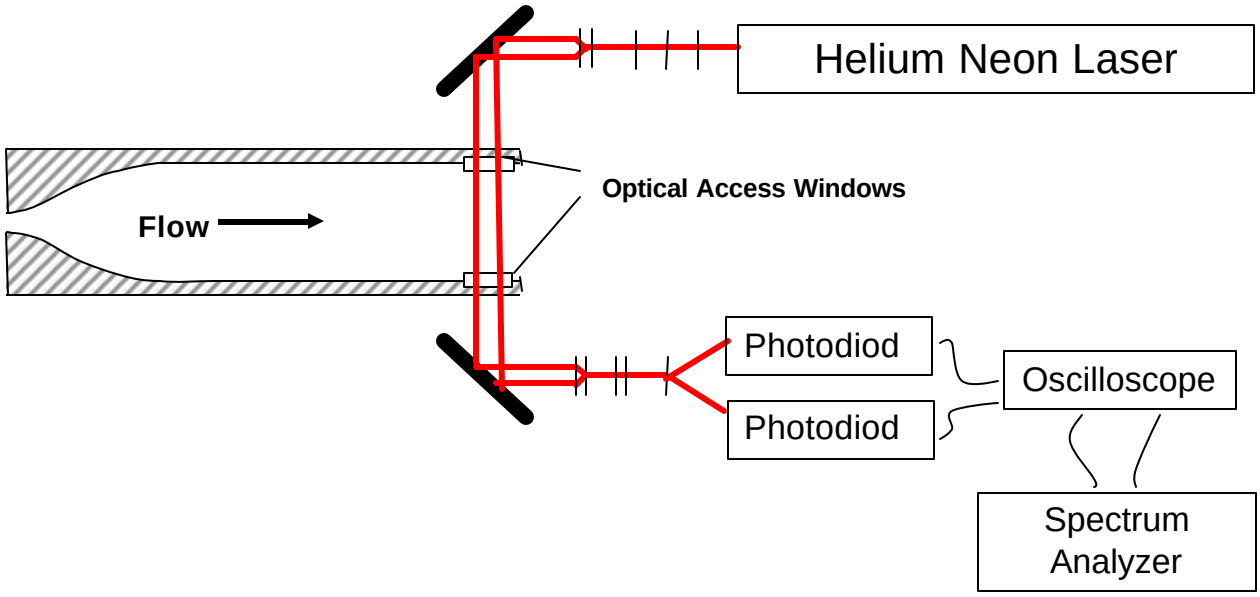

Figure 11: Schematic showing how the LDI is integrated into the experimental apparatus

Figure 12 shows the location of the LDI reference beam and test locations of the probe beam. The beams are superimposed on a schlieren image of the same flow. The central region of the figure is an image of the flow seen through the optical access windows, with the lighter regions representing the boundary layer. Pitot tube measurements indicate that the boundary layer extends approximately 8 mm into the flow [5]. The relative positions of the test locations are as follows: the test location near the wall is approximately 1-2 mm from the wall, the test location midway through the boundary layer is approximately 4-5 mm from the wall, and the test location in the center of the flow is approximately the same distance from the wall as the reference beam.

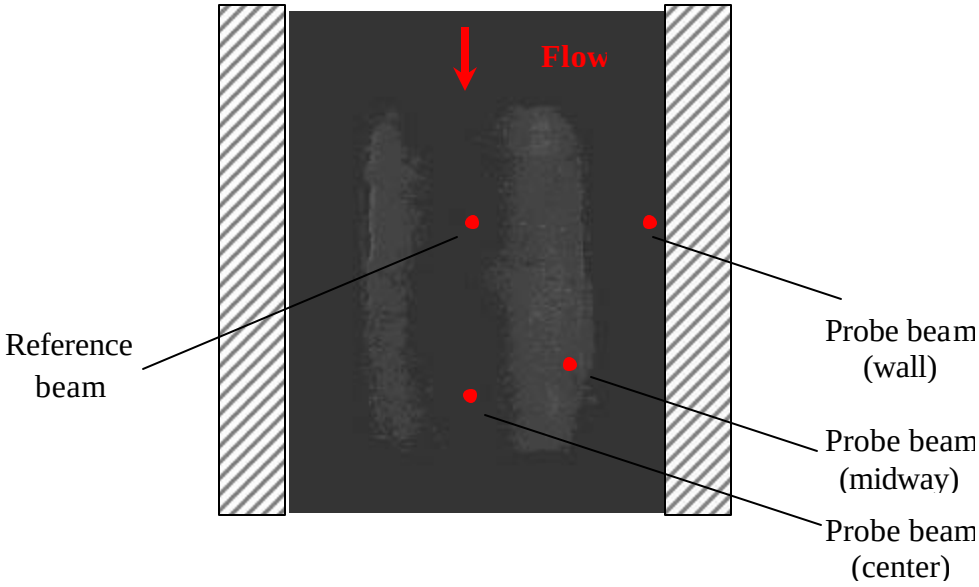

Figure 12: Beam locations on a schlieren image of the flow

Results

The run-to-run signal intensity of the LDI spectra varies, but the shape of the spectra is very reproducible. Since the measurements are plotted on a log-x scale, the curves are normalized at the end of the roll-off where the density of data points is at its highest. When measurements of the flow under the same conditions are normalized and plotted together, the observed disparity is less than 1 dB.

Theoretical calculations suggest that the flow regime in both wind tunnels is turbulent. An attempt was made to verify this using the LDI. The mass flow rate and stagnation pressure were varied in an attempt to observe a dramatic change in the spectra, but no such phenomenon was observed. A small strip of sandpaper was glued to the larger dimension wall in the throat to trip the boundary layer in case the flow was laminar, but the spectra did not significantly change.

Experiments have been conducted with and without a ceramic honeycomb flow straightener located in the nozzle plenum. Nitrogen gas enters the rectangular wind tunnel through 1" nominal diameter plastic tubing which is larger than the 2 cm width of the wind tunnel. This results in flow velocity vectors that are not parallel, creating pressure and density variations at the onset of the wind tunnel. The honeycomb essentially converts this single jet into several hundred smaller jets which helps align the velocity vectors streamwise, resulting in reduced pressure and density variations across the flow. The honeycomb has 400 holes per square inch and is 1" long. Figure 13 compares LDI measurements taken with and without the honeycomb in place, and shows that the honeycomb significantly attenuates density fluctuations occurring below 7 kHz while increasing density fluctuations occurring above 7 kHz. This suggests that large scale flow structures are broken up into smaller scale structures. The LDI measurements taken with the honeycomb installed in the wind tunnel are qualitatively consistent with the flight measurements shown in Figure 4 [6].

Figure 14 shows LDI spectra measured with the probe beam at the wall, midway through the boundary layer, and in the core of the flow. The density fluctuations are highest midway through the boundary layer and lowest in the core of the flow. These results are consistent with hypersonic boundary layer spectra measurements in Reference [6].

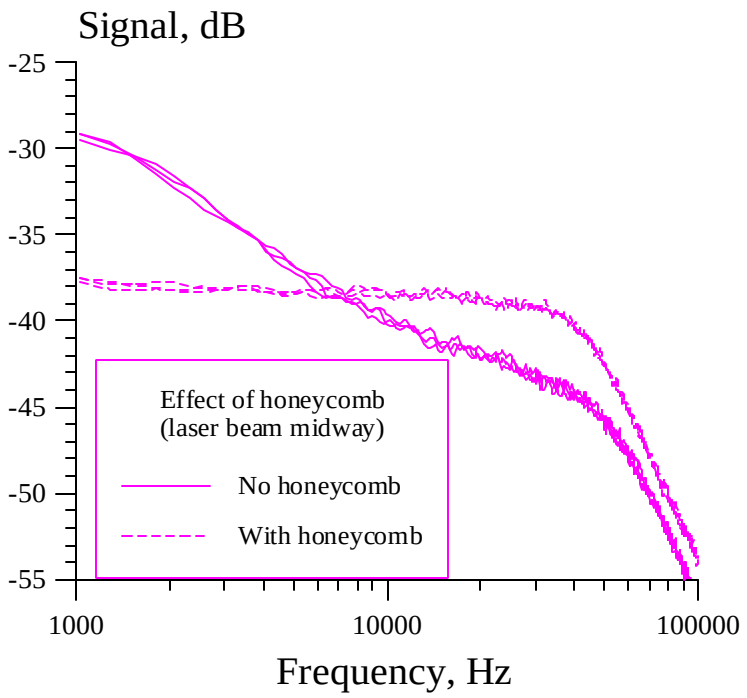

Figure 13: LDI spectra in M=3 nitrogen flows with a 250 torr stagnation pressure in the first test section. Three cold flow measurements are shown for flows with and without the honeycomb. The probe beam is located midway through the boundary layer.

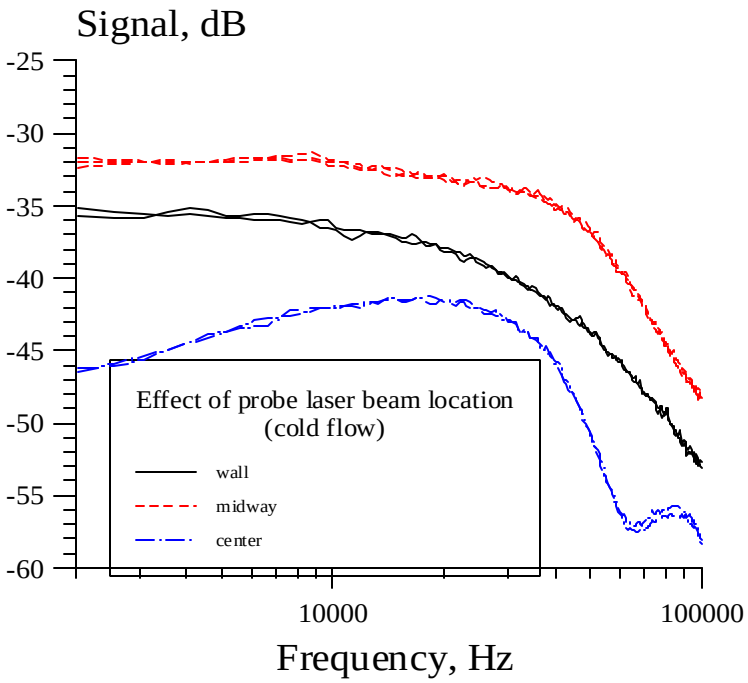

Figure 14: LDI spectra in M=3 nitrogen flows with a 250 torr stagnation pressure in the second test section. Two conditions are shown for probe beam locations near the wall, midway through the boundary layer, and in the center of the flow.

Figure 15 shows LDI spectra of M=3 nitrogen flows for four experimental configurations: cold flow, plasma with magnetic field, plasma with crossed electric and magnetic fields producing an accelerating MHD force, and plasma with crossed electric and magnetic fields producing a decelerating MHD force. In all cases, the probe beam traversed the flow midway through the boundary layer. The measurements taken at each experimental configuration have been shifted for illustrative purposes. Note that the shapes of curves are very reproducible. The signal spike at 90 kHz was determined to be noise from the DC power supply. The spike was somewhat drowned out in stronger spectrums and appeared large in weaker spectrums.

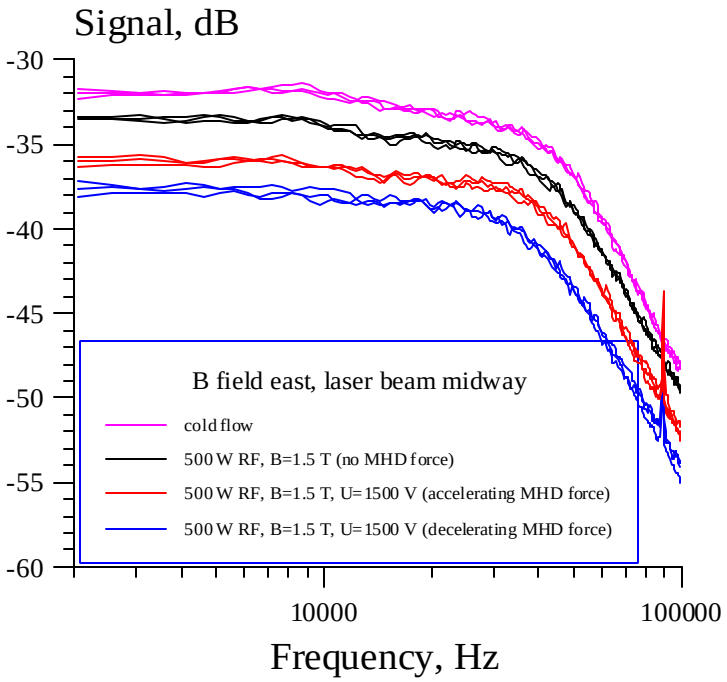

Figure 15: LDI spectra in M=3 nitrogen flows with a 250 torr stagnation pressure in the first wind tunnel. Three measurements were taken for each configuration. The probe beam was located midway through the boundary layer.

Figure 16 shows the cold flow (purple) and ionized flow (black) measurements from Figure 15, but with the curves normalized. There does not appear to be distinguishable differences in the measurements, which suggests that the effect of Joule heating on the flow is negligible.

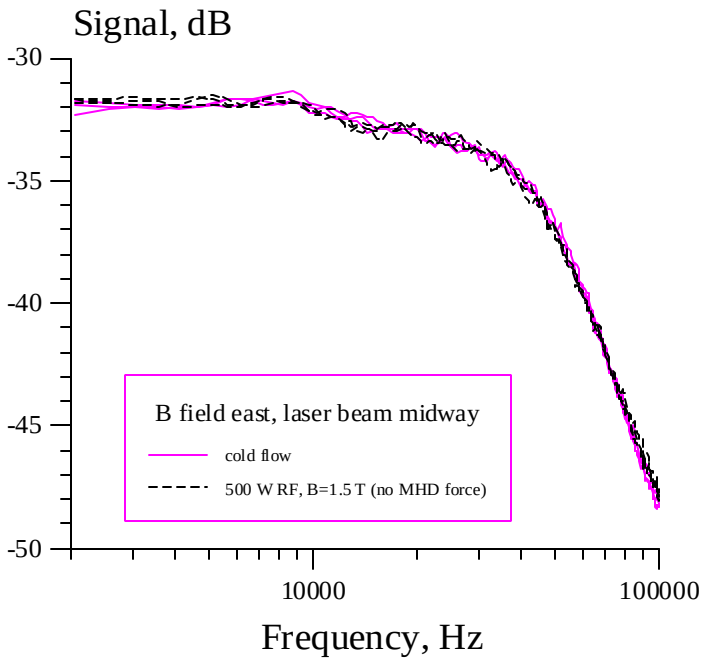

Figure 16: Cold flow and plasma flow measurements of Figure 15 normalized at the roll-off. There is not a distinguishable difference between the measurements, so Joule heating is considered negligible.

Figure 17 shows the measurements of Figure 15 that produce an accelerating (red) and decelerating (blue) MHD force, but with the curves normalized. In the frequencies up to the roll-off, the difference between each configuration is between 1-2 dB. The MHD effect is predominately observed between 10-30 kHz.

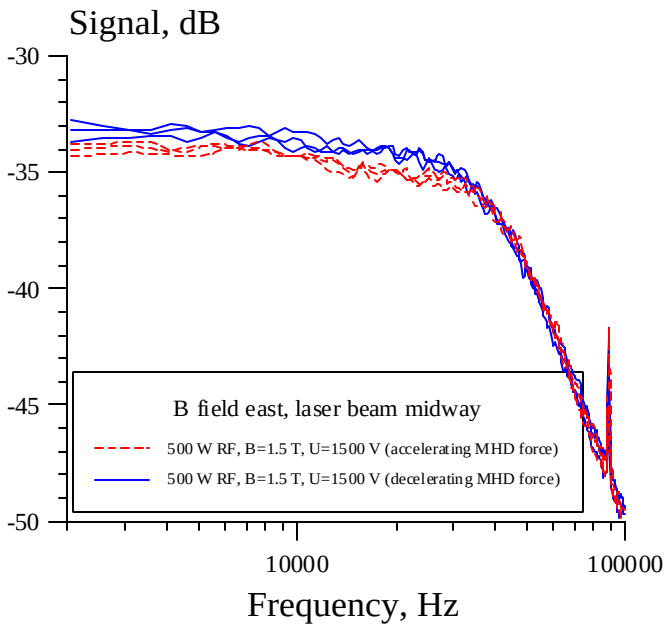

Figure 17: Measurements from Figure 15 that produce accelerating and decelerating MHD forces normalized at the roll-off. The MHD affect is observed.

Figures 18-20 repeats the data analysis of Figures 15-17 with the probe beam near the wall in the second wind tunnel.

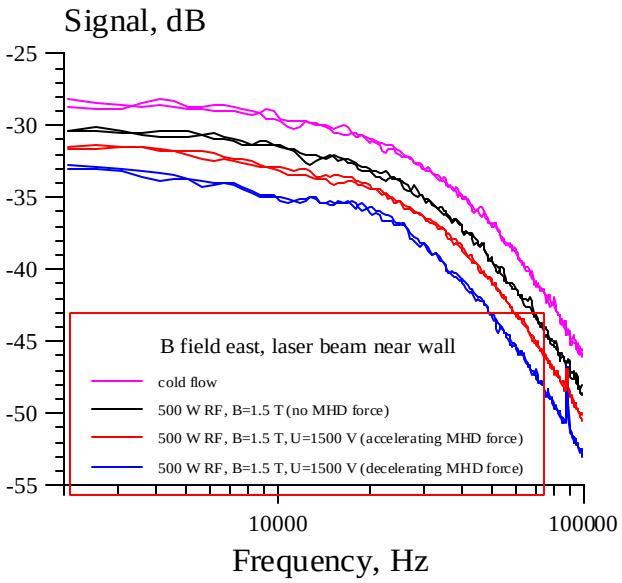

Figure 18: LDI spectra in M=3 nitrogen flows with a 250 torr stagnation pressure in the second wind tunnel. Three measurements were taken for each configuration. The probe beam was located near the wall of the wind tunnel.

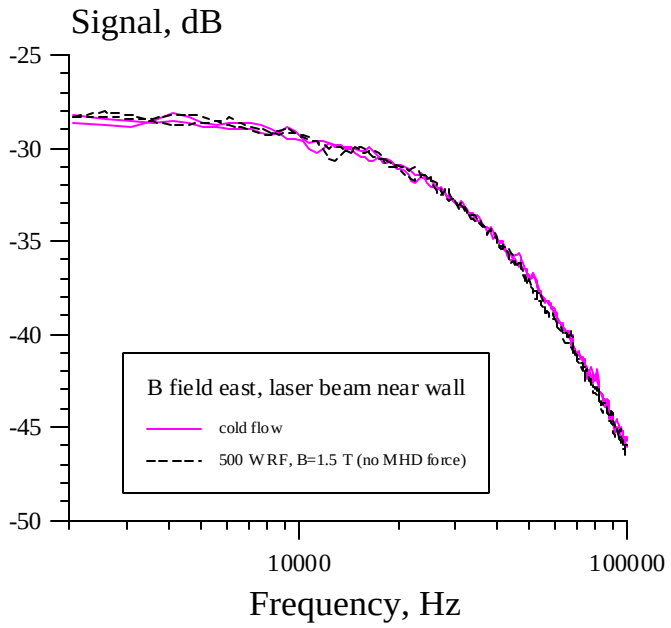

Figure 19: Cold flow and plasma flow measurements of Figure 18 normalized at the roll-off. There is not a distinguishable difference between the measurements, so the negligible effect of Joule heating is verified.

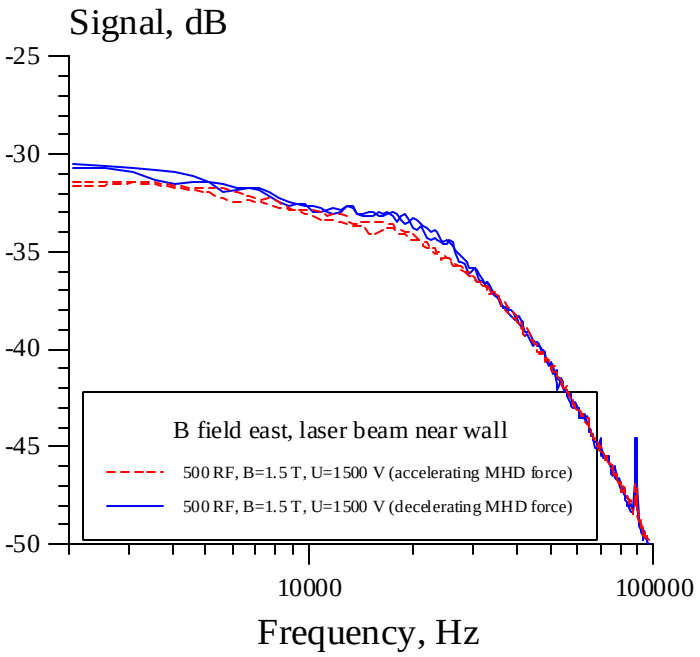

Figure 20: Measurements from Figure 18 that produce accelerating and decelerating MHD forces normalized at the roll-off. The MHD affect is observed.

The MHD force can be induced through four different experimental configurations; two configurations produce an accelerating MHD force, and two configurations produce a decelerating MHD force. These four configurations are achieved by switching the polarity of the DC and magnetic fields. For one DC field polarity, an accelerating and decelerating MHD force can be produced by switching the polarity of the magnet. Alternatively, for one magnet polarity, an accelerating and decelerating MHD force can be produced by switching the polarity of the DC field.

Figure 21 shows the MHD effect in four experimental configurations; two configurations producing an accelerating MHD force, and the other two producing a decelerating MHD force. These results verify that the direction of the MHD force, and not the application of the applied electric and magnet fields, is causing the flow alteration.

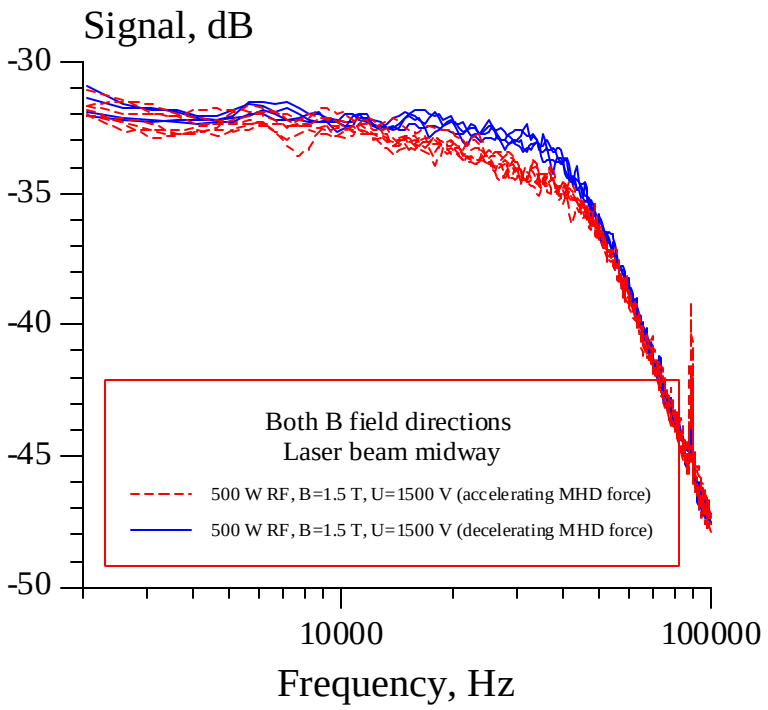

Figure 21: LDI spectra in M=3 nitrogen flows with a 250 torr stagnation pressure in the first wind tunnel. Probe beam is midway through the boundary layer. Six measurements of spectra with a decelerating MHD force from two experimental configurations are plotted with four measurements of spectra with an accelerating MHD force from two experimental configurations.

An MHD force effect has been observed in two wind tunnels. Joule heating was found to have a negligible influence on the density fluctuations in the flow. The application of the applied electric and magnetic fields did not affect the flow.

Conclusions

An LDI has been constructed to measure density fluctuations in two M=3 wind tunnels. The systems bandwidth, sensitivity, and response time have been determined to be exceedingly adequate for spectra measurements between 0-102.5 kHz. The LDI has been integrated into the experimental apparatus using beam directing optics. Although the run-to-run intensity of the LDI measurements varies, the shapes have very good reproducibility. This was verified by graphically normalizing the signals and examining the results.

Measurements have been taken on cold flows and the results are consistent with past work. In particular, the turbulence intensity in the boundary layer was found to increase with distance from the wall. The turbulence intensity in the free stream of the flow was found to be smaller than the turbulence intensity near the wall of the wind tunnel. The general form of the LDI measurements and the location of the roll-off also appear to be consistent with past experiments.

The flow was ionized using an RF discharge and a transverse current was drawn in the flow using a DC power supply in the presence of a B=1.5 T magnetic field. The MHD effect has been observed in two different wind tunnels running nitrogen flows. In both wind tunnels, the effect of Joule heating was shown to be negligible. The MHD effect was observed near the wall and midway through the boundary layer in the second wind tunnel, and midway through the boundary layer in the first wind tunnel (could not test near the wall in this wind tunnel because of the location of the optical access windows). The accelerating MHD force produced a well reproduced reduction in density fluctuations, while the decelerating MHD force produced a well reproduced increase in density fluctuations. The difference in density fluctuation intensities between measurements with accelerating and decelerating MHD force configurations reached up to 10-20% (1-2 dB). This effect was observed for two different experimental configurations producing one direction of the MHD force, which suggests that the application of the fields has an insignificant affect on the spectra.

Future Work

The flow regime of both test sections is a current area of interest. Flow visualization will be accomplished using a second laser-based diagnostic instrument that utilizes laser light-scattering. Pulsed laser sheets will pass through the flow (parallel or orthogonal to the flow direction) and light will scatter off of small water droplets that form in the flow due to condensation. A CCD camera will be positioned to capture images of the scattered light. These images will be compared for changes in flow structures. If the condensation does not form quickly enough in the test section, the flow will be seeded with acetone to stimulate it.

The current results will also be verified using an alternative power supply to ionize the flow. A pulsar power supply will be substituted for the RF power supply and experiments will be repeated. This method of ionization is expected to increase the flow's conductivity, which would amplify the MHD effect on the flow.

References

1. Henoch, C., and Stace, J., "Experimental Investigation of a Salt Water Turbulent Boundary Layer Modified by an Applied Streamwise Magnetohydrodynamic Body Force," Phys. Fluids, vol. 7, no. 6, 1995, pp. 1371-1383
2. Salyer, T. R., Collicott, S. H., and Schneider, S. P., "Feedback Stabilized Laser Differential Interferometry for Supersonic Blunt Body Receptivity Experiments," AIAA-2000-0846, 38th AIAA Aerospace Sciences Meeting and Exhibit, Reno, NV, Jan. 2000
3. Belcher, P. M., "Predictions of Boundary Layer Turbulence Spectra and Correlations for Supersonic Flight", 8 Congres International D'Acoustique, Liege, 7-14 September 1965
4. Meyer, R., Chintala N., Bystricky, B., Hicks, A., Cundy, M., Lempert, W. R., and Adamovich, I. V., "Lorentz Force Effect on a Supersonic Ionized Boundary Layer", AIAA Paper 2004-0510, January 2004
5. R. Meyer, B. McEldowney, N. Chintala, P. Palm, and I. V. Adamovich, "Experimental Studies of Plasma Assisted Ignition and MHD Supersonic Flow Control", AIAA Paper 2003-0873, presented at 41st Aerospace Sciences Meeting and Exhibit, January 2003, Reno, NV
6. K. F. Stetson, E. R. Thompson, J. C. Donaldson, and L. G. Siler, "Laminar Boundary Layer Stability Experiments on a Cone at Mach 8. Part 1: Sharp Cone", AIAA Paper 83-1761, presented at AIAA 16th Fluid and Plasma Dynamics Conference, July 1983, Danvers, MA